Comparing Evaporative Sources of Terrestrial Precipitation and Their Extremes in MERRA Using Relative Entropy

Paul A. Dirmeyer[1,2], Jiangfeng Wei[3], Michael G. Bosilovich[4], and David M. Mocko[4,5]

[1] Department of Atmospheric, Oceanic and Earth Sciences, George Mason University, Fairfax, Virginia, USA

[2] Center for Ocean-Land-Atmosphere Studies, Institute of Global Environment and Society, Calverton, Maryland, USA

[3] Jackson School of Geosciences, University of Texas at Austin, Austin, Texas, USA

[4] Global Modeling and Assimilation Office, NASA Goddard Space Flight Center, Greenbelt, Maryland, USA

[5]SAIC, Greenbelt, Maryland, USA

Submitted to *Journal of Hydrometeorology*
23 July 2014

Abstract:

A quasi-isentropic back trajectory scheme is applied to output from the Modern Era Retrospective-analysis for Research and Applications and a land-only replay with corrected precipitation to estimate surface evaporative sources of moisture supplying precipitation over every ice-free land location for the period 1979-2005. The evaporative source patterns for any location and time period are effectively two-dimensional probability distributions. As such, the evaporative sources for extreme situations like droughts or wet intervals can be compared to the corresponding climatological distributions using the method of relative entropy. Significant differences are found to be common and widespread for droughts, but not wet periods, when monthly data are examined. At pentad temporal resolution, which is more able to isolate floods and situations of atmospheric rivers, values of relative entropy over North America are typically 50-400% larger than at monthly time scales. Significant differences suggest that moisture advection may be key to precipitation extremes. Where evaporative sources do not change significantly, it implies other local causes may drive the extremes.

1. Introduction

Rain or snow falling over any particular location is composed of condensed water vapor that entered the atmosphere as surface evaporation from a range of upstream locations. Surface and atmospheric conditions along the paths of moisture advection determine the ultimate sources of evaporative moisture, which generally have a combination of oceanic and terrestrial origins. Knowledge of the sources of moisture supplying precipitation over a particular location could be used to understand how upstream surface changes may affect local hydrology, and potentially to aid prediction (e.g., Dirmeyer and Kinter 2010; Bagley et al. 2012, Spracklen et al. 2012).

There are three basic approaches to estimating the connection between surface evaporation from specific locations and subsequent precipitation of that water. The simplest but most limited in capabilities is the bulk method, which relies on regional atmospheric moisture budgets at relatively long time scales, typically one month (Brubaker et al. 1993). This approach is most often used to estimate precipitation recycling as derived by Budyko (1974) – the portion of precipitation over a given area that originated as evaporation within the same area (e.g., Eltahir and Bras 1994, Gong and Eltahir 1996, Trenberth 1999). Burde et al. (1996) showed that this method has an implicit assumption of one-dimensionality that causes errors, which can be accounted for in a two-dimensional derivation, further refined by Burde and Zangvil (2001). These approaches typically use global atmospheric reanalyses as the source of the necessary meteorological fields. Dominguez et al. (2006) recognized the lack of water budget closure in reanalyses could affect the bulk

estimates, but decided the impact was small over the United States. Bisselink and Dolman (2008) came to the same conclusion for Europe. This approach has been extended to differentiate solely between terrestrial and oceanic moisture sources (e.g., Gimeno et al. 2010; Goessling and Reick 2011). van der Ent (2010) developed a backtracking model based on the vertically-integrated moisture transport and the constraints of atmospheric water balance, but still in the Eulerian framework. Keys et al. (2012) developed an interesting variant on that approach to estimate the "precipitation-sheds" of regions, to assess their potential vulnerability to changing evapotranspiration with land use changes.

Another approach is to include water vapor tracers directly within a three-dimensional model of the atmosphere. This approach typically accomplishes the tracing in a Lagrangian framework, providing a highly accurate set of trajectories for water vapor parcels. Druyan and Koster (1989) tagged water vapor evaporation from specific regions in a global model to compare moisture sources during wet and dry conditions over the Sahel. Bosilovich and Sun (1999) performed a similar analysis with a regional model over the central United States. Numaguti (1999) performed a continental-scale tracer analysis over Eurasia, while Bosilovich and Schubert (2002) performed a global study of evaporative sources of precipitation using tracers in a global atmospheric model. Stohl and James (2004) used a dispersion model driven by reanalyses to examine a case study of moisture transport over Europe, and a one-year global assessment. Stohl and James (2005) applied the method to diagnose oceanic moisture sources to major river basins.

A variation on the tracer approach is to use water isotopes as the markers (Henderson-Sellers et al. 2004). Terrestrial versus oceanic sources can be distinguished in this manner. Kurita et al. (2004) were able to trace the changing sources of precipitable water across Russia from isotope measurements. Salati et al. (1979) did this for the Amazon basin, and Tian et al. (2001) measured the northward penetration of the South Asian monsoon circulation over Tibet using isotopic measurements, among many other regional studies. An atmospheric isotope model was employed by Yoshimura et al. (2004) in a study of moisture sources for the Asian monsoon.

The bulk approaches mentioned above suffer several shortcomings, including errors introduced by the coarse temporal and vertical resolution of the methodology and data, lack of water budget closure in reanalysis data sets, and neglect of nonlinear processes and asymmetrical moisture advection. Tracers embedded within atmospheric models can have "perfect" tracking of water vapor at the full spatial and temporal resolution. However, they tend to add great expense to the simulations, especially in terms of computer memory use and data storage, as each additional evaporative source requires another full three-dimensional state variable to be carried in the model and integrated forward in time. Also, calculations from these methods are subject to all the systematic errors of the model, which can often be substantial for quantities like precipitation and evaporation (Kanamitsu et al. 2002). Models can be constrained by data assimilation, but the assimilation of humidity violates conservation and closure of the water budget, which cannot be handled elegantly by tracers.

A compromise is to calculate the tracers a posteriori from atmospheric analyses at a high spatial and temporal resolution that resolves the synoptic-scale fluctuations in water vapor, and even the diurnal cycle, as well as the vertical structure of moisture in the atmosphere, but may not use data from every time step of the atmospheric model producing the analysis. When using reanalyses as the source of the meteorological forcing data, the issue of lack of closure of the water budget still arises, but is less severe, particularly when observed precipitation data are used to constrain the model simulations. This method has been used to independently validate other methods of estimating precipitation recycling and its variability (Brubaker et al. 2001; Sudradjat et al. 2003; Dirmeyer and Brubaker 2007), define regional links between tropical moisture and mid-latitude floods (Dirmeyer et al. 1999; Reale et al. 2001; Sudradjat 2002; Turato et al. 2004; Dirmeyer and Kinter 2009, 2010, Wei et al. 2012), quantify links between nations through the atmospheric branch of the hydrologic cycle (Dirmeyer et al. 2009), estimate remote impacts of tropical land use change (Bagley et al. 2012) and study the fate of evaporated irrigation water (Tuinenburg et al. 2012; Wei et al. 2013).

In this paper, we present results of this type of approach, the quasi-isentropic back-trajectory scheme of Dirmeyer and Brubaker (2007) applied globally at a higher spatial resolution than it has been previously, using NASA reanalysis products. In addition to determining sources of evaporated moisture supplying precipitation and estimating recycling ratios, differences in the distribution of sources during droughts and wet intervals are quantified.

Section 2 describes the data sets used, the back-trajectory technique that estimates the distribution of evaporative sources for moisture supplying precipitation over any location, and a robust statistical method to compare distributions of evaporative sources. The basic distributions of moisture sources are presented in Section 3. Section 4 investigates how source regions vary in the cases of precipitation extremes. Discussion is presented in Section 5.

2. Data and Methods

The global meteorological analysis used for this study is the Modern Era Retrospective-analysis for Research and Applications (MERRA; Rienecker et al. 2011). MERRA uses the Goddard Earth Observing System (GEOS-5) atmospheric model and data assimilation system at a resolution of 2/3° longitude by 1/2° latitude, overlying the Catchment land model (Koster et al. 2000; Ducharne et al. 2000). MERRA placed an emphasis on improved simulation of the global hydrologic cycle, assimilating instantaneous precipitation rates (Decker et al. 2011). Nevertheless, model biases and discontinuities from changing satellite platforms introduce precipitation errors (Robertson et al. 2011), which affect the surface water budget.

Reichle et al. (2011) used the replay feature of GEOS-5 to generate a land-only analysis called "MERRA-Land", where precipitation from the observationally based Global Precipitation Climatology Project (GPCP; Huffman et al. 2009, Xie et al. 2003) is used to correct MERRA precipitation. This results in estimates of evaporation and

131 other surface quantities that are more consistent with observations. Dirmeyer
132 (2011) showed that MERRA-Land surface flux data produce estimates of land-
133 atmosphere coupling that are much more consistent with a wide range of other data
134 sets than MERRA.

135 These data are used to drive the quasi-isentropic back trajectory scheme that
136 estimates the distribution of surface evaporation that supplies precipitation as a
137 function of space and time (Brubaker et al. 2001; Dirmeyer and Brubaker 2007). It
138 is a Lagrangian method that traces the advection of moisture back in time from
139 precipitation events, and uses upstream evaporation and precipitable water
140 estimates to determine the probabilistic distribution of surface evaporation
141 supplying the precipitated water vapor to the atmosphere. Data are aggregated in
142 time over 5-day and monthly intervals, with a spatial distribution for every land
143 surface grid point. On a high-resolution global grid such as MERRA, this generates a
144 very large set of two dimensional source fields. The source fields for a set of grid
145 boxes, delineating a river basin, nation, or any arbitrary land area, can be easily
146 calculated by aggregation from the resolution grid.

147 The spatial pattern of surface evaporative sources is effectively a two-dimensional
148 probability distribution. There exist objective quantitative methods to determine
149 the degree of similarity between two probability distributions. Relative entropy,
150 which also goes by other names such as information divergence and Kullback
151 Leibler divergence, is such a quantification (cf. DelSole and Tippett 2007). The
152 relative entropy between two distributions p and q on a discrete spatial grid is
153 defined as (Kleeman 2002):

154 $$RE_{p,q} = \sum_i p(i) \log \frac{p(i)}{q(i)}$$

155 where *i* is the index of the grid points (in our case it is two dimensional but it applies
156 over any number of dimensions) and each of the distributions are defined as having
157 a sum total of unity. Thus, we must normalize any spatial distributions before
158 applying this method. For two identical distributions, *RE*=0. Any deviations will
159 increase the value of *RE*. $RE_{p,q} \neq RE_{q,p}$, but the ranking is preserved with either
160 choice of *p* and *q*, and *RE* is invariant to linear and nonlinear transforms.

161 What is not straightforward, however, is quantification of a statistical significance in
162 the difference between two distributions when they do not share identical or well-
163 described low-order moments (DelSole and Tippett 2007). For example, the
164 significance in the shift between two normal distributions can be quantified, but if
165 one or both distributions are non-normal, or otherwise do not share basic shape
166 parameters, significance can only be determined by Monte-Carlo bootstrap
167 techniques. We have used such an approach, which is described in the next section
168 along with some characteristics of the climatology of evaporative sources.

169

170 **3. Evaporative Sources**

171 Figure 1 shows the total evaporative source supplying precipitation over land
172 (Antarctica and other ice-covered points excluded) aggregated from monthly data
173 for each season. Two sets of estimates are used; one based on MERRA with
174 precipitation corrected by GPCP and MERRA-Land estimates of evaporation (top
175 panels), as well as one based solely on the original MERRA output. The bottom

176 panels show the difference between evaporative source estimates with MERRA
177 alone minus the estimates where MERRA-Land is used for terrestrial evaporation
178 and precipitation estimates. Looking first at the top panels, there is a clear
179 seasonality to both the terrestrial and oceanic sources of evaporation supplying
180 precipitation over land. The strongest sources tend to be in low latitudes over land
181 and adjacent open oceans, although a number of areas in the northern mid-latitudes
182 become prominent in JJA. The strength of oceanic sources correlate strongly to the
183 distance to shore, but there are exceptions (e.g., the closed 30 kg m^{-2} contour in the
184 North Pacific during JJA).

185 The bottom panels of Fig 1 show that MERRA evaporation (and precipitation) over
186 land is generally much higher than GPCP observations suggest should be the case.
187 Yet, MERRA has a very strong cross-equatorial gradient in terrestrial precipitation,
188 with erroneously dry conditions over much of South America and Africa. These
189 systematic errors greatly impact the estimates of evaporative sources – motivating
190 our use of MERRA-Land for our calculations. The fraction of evaporated moisture
191 feeding precipitation over the land areas in the top panels is 52%, 62%, 50% and
192 45% during MAM, JJA, SON and DJF respectively. When the MERRA output with its
193 precipitation biases is used to estimate evaporative sources, the terrestrial
194 percentages increase to 55%, 64%, 52% and 46%.

195 Figure 2 gives a notion of how regional evaporative sources appear. The mean
196 surface evaporative sources supplying precipitation to four sections of the
197 conterminous United States are presented, normalized to indicate the percentage of
198 the total supplied from each MERRA grid box. This and all future figures are based

on the estimates using the corrected precipitation and MERRA-Land evaporation. The source into the western U.S. is seen to have a long fetch stretching from the subtropical North Pacific, indicative of the "atmospheric rivers" that supply much of the moisture for winter rain and snow (e.g., Dettinger et al. 2011). There is also a great deal of moisture supplied from terrestrial evapotranspiration over northern California, Oregon and Washington, according to this analysis.

The Great Plains and eastern Rockies have an evaporative source that mainly comes from the western Gulf of Mexico, as well as terrestrial areas in the southern part of the region, and sporadic moister localities across the inter-mountain West. The region of the Pacific off the coast of Baja California is also a moisture source prior to the onset of the North American monsoon (cf. Brubaker et al. 2001).

The bottom panel of Fig 2 shows the evaporative source supplying precipitation over the states of the Mississippi Basin mainly east of the Great Plains. This area also shows a major oceanic source from the Gulf of Mexico, but with more extent into the northern Caribbean Sea (cf. Dirmeyer and Kinter 2010), and little moisture coming from the west. There is again a substantial terrestrial source over the southern and central portions of the area.

The top panel also shows the evaporative source for the East Coast, which shows much more of a source from the open Atlantic than does the Mississippi Basin area. Again, little moisture supplying precipitation comes from the west – most comes from the south. Recycling over each area, defined as the fraction of the total evaporative moisture source that lies within the boundaries of the region, are 12%, 22%, 19% and 14% for the West, Great Plains, Mississippi Valley and East Coast

222 respectively. For the same regions, oceanic moisture sources account for 81%, 48%,
223 46% and 53% of precipitation.

224 Figure 3 shows for each season the fraction of precipitation at each grid point that
225 originated from evaporation over land. The pattern of mean low-level flow is
226 evident in the patterns. In mid-latitudes, where winds are predominantly from the
227 west, the west coasts receive predominantly moisture of oceanic origin, and the
228 eastern sides of continents have much more moisture of terrestrial origin. The
229 pattern is reversed at low latitudes. The global mean fractions of terrestrial sources
230 of moisture supplying terrestrial precipitation are 46%, 50%, 40% and 38% during
231 boreal spring, summer, fall and winter respectively.

232 There are also some pronounced regional seasonal cycles. Large areas of central
233 Asia into Siberia receive more than 90% of their precipitation from land
234 evaporation during spring and summer. The region around Ethiopia and Sudan has
235 a large oscillation between oceanic sources in the winter and spring, and terrestrial
236 sources during summer into fall. Much of southern Africa has a similar variation,
237 but six months out of phase. The general east-west gradient over North America is
238 maintained through out the year, but fluctuates from a predominance of marine
239 sources in winter to a much larger portion of continental sources in summer. Most
240 of Eurasia also shows the same annual cycle as North America.

241 Very strong gradients are evident across the steep terrain of the Himalayas, with
242 large terrestrial proportions over the Tibetan Plateau, and predominant oceanic
243 sources to the south. This gradient extends northeastward across China. There are
244 also fairly strong gradients along the Rift Valley of Africa, but curiously there is little

245 apparent signature of the Rocky Mountains or Andes except in the immediate
246 vicinity of the Altiplano.

247 The distance from each terrestrial grid point to the central moment of the
248 climatological evaporative source is shown in Fig 4. This gives an indication of the
249 average distance water vapor travels in the air before falling as rain or snow at that
250 location. Arid regions far from open ocean typically have the largest values, with
251 substantial areas of the Sahara (all seasons) and south-central Asia (all except JJA)
252 showing values in excess of 4000km. The shortest fetches are found in subtropical
253 regions during the local rainy season. Parts of subtropical South America, southern
254 Africa and northwestern Australia show typical distances of less than 500km, as
255 does a band across the Sahel to Ethiopia, particularly during JJA. These areas show
256 some persistence of the relatively short transport distances even in the dry season.
257 Surprisingly, the distances are somewhat longer in the deep tropics. The effect of
258 the annual cycle of winds and terrestrial evaporation are evident over the middle
259 and high latitudes of the Northern Hemisphere. Distances are shorter in the
260 summer when land evapotranspiration is greatest and winds are lighter.

261 The remainder of the paper discusses the quantification of evaporative sources
262 associated with hydrologic extremes. To do so requires quantification of the
263 deviation of an evaporative source from its climatology. The method of relative
264 entropy was described in Section 2. Figure 5 shows the average value of the relative
265 entropy calculated between the climatological pattern of evaporative sources and
266 each of the 27 individual years, on a monthly basis then aggregated to seasonal,
267 calculated for every land grid point. Small values suggest there is very little

268 variation in the probability distribution, represented by the normalized evaporative
269 source like those depicted in Fig 2 for area totals. Small values predominate over
270 the tropics, monsoon regions during the wet season, and humid regions in general.
271 Large values are most likely over arid regions, suggesting a great deal of interannual
272 variability in moisture sources there.

273 However, there is not a one-to-one correspondence between precipitation and the
274 interannual variability in moisture sources. For example, northern Australia shows
275 very large RE values during MAM and a minimum during SON, even though DJF is
276 the wet season and JJA is the core of the dry season. Likewise, over the western
277 Great Plains there is a clear maximum in relative entropy, and thus peak year-to-
278 year variability in moisture sources, during SON, which is a period of transition from
279 a late spring peak to a winter minimum in total precipitation.

280

281 **4. Extremes**

282 The relative entropy statistic provides a handy measure of the difference between
283 any two patterns of evaporative sources. As an example of the application of the
284 relative entropy calculation, the differences between the global estimates of
285 evaporative sources of terrestrial precipitation shown in Fig 1 result in relative
286 entropies of 0.30, 0.76, 0.37 and 0.14 for MAM, JJA, SON and DJF respectively. This
287 quantifies what can be seen by eye, that the largest differences appear during JJA,
288 and the two estimates for DJF are rather similar on a global scale.

289 Here, we use relative entropy to determine the difference from the climatological
290 pattern of evaporative sources at each land grid point for specific climatic
291 categories, namely the months and years with the greatest or least precipitation.
292 With this approach, we may determine whether changes in the sources of moisture
293 supplying precipitation (i.e., changes in circulation, moisture advection, and remote
294 evaporation) are significant contributors to precipitation extremes. For locations
295 where the answer is negative, other causes may be at play, such as local conditions
296 like atmospheric stability, convective potential or land surface feedbacks, or
297 possibly other large-scale factors not discernable from our back-trajectory analysis.

298 Figure 6 shows the relative entropy calculated at each point between the
299 evaporative source averaged over just the three driest years, based on GPCP
300 precipitation, and the 27-year climatological evaporative source. The calculation is
301 performed on the lower-resolution GPCP data grid, and only differences significant
302 at the 90% confidence level are shown. Significance is estimated by a Monte Carlo
303 method, where the mean evaporative source and that for each of the 27 individual
304 years, for each season, are used to calculate relative entropies, and the mean and
305 standard deviation of the 27 values are calculated at each point. This is then
306 compared to the same calculations made for each combination of 3 years, a sample
307 size of 2,925, but only for a subsample of 100 points and seasons (computational
308 expense is otherwise prohibitive). Assuming the variability of relative entropy is
309 normally distributed, and that a linear transform can be used for the means and
310 standard deviations between the combinations of 27 taken three at a time and
311 combinations of 27 taken one at a time, we scale the significance thresholds.

312 The largest values of relative entropy are over arid and semi-arid regions,
313 suggesting when these areas suffer drought, there are large changes in the pattern
314 of evaporative moisture sources. Humid areas show smaller values, and thus
315 smaller absolute variations in the patterns of evaporative moisture sources.
316 However, the areas of significant variations are widespread and not limited to any
317 specific climate regime. Nevertheless, some general patterns emerge. During DJF,
318 there is little significant connection between changing moisture sources and
319 drought across the Southern Hemisphere. Summer is also the season with the least
320 coverage of significant moisture transport across most of the Northern Hemisphere.
321 At high latitudes in winter, changing moisture sources are significant. This is
322 consistent with the strong limitations on precipitable water in the Clausius
323 Clapeyron relationship; in cold regions and seasons, precipitation is strongly
324 correlated with temperature, which is often tied to prevalent wind direction. We
325 also see that monsoon regions in North America and Asia, and to a lesser extent
326 Africa, show significant relative entropies in the transition seasons, where late
327 onsets or early retreats of monsoon rains seem to be connected to circulation
328 anomalies.

329 The same relative entropy calculations were performed for the three wettest years
330 at each location, shown in Fig 7. Here we find few points with statistically
331 significant changes in evaporative sources. The reason for this is straightforward.
332 Whereas droughts are the result of a deficit of precipitation over an extended period
333 of time, typically several months or more, floods often result from one or a few very
334 heavy precipitation events occurring over brief periods of days. A wet month or

season could be the result of an anomalous moisture source, like that brought by "atmospheric rivers", which lasts only a few days. These events can easily become lost when monthly or seasonal statistics are calculated.

Seasonal mean values of relative entropy were recalculated using the original pentad-by-pentad estimates of evaporative sources over a portion of North America. The results for the three wettest cases, based on pentad GPCP precipitation data, are shown in Fig 8. No significance test has been applied. In all seasons, changes in the evaporative source are a larger factor in flood events over the mountainous areas of the West and over much of Canada than the rest of the United States. Spring is the peak season for circulation changes to be associated with floods over the eastern U.S. Over the North American monsoon region, relative entropy peaks during spring and reaches a minimum in fall.

The impact of the choice of time scale is clearly evident in Fig 9. The figure shows the natural logarithm of the ratio of the relative entropy at each point – pentad versus monthly. Positive values dominate, indicating that changes in the evaporative source regions are more of a factor in precipitation anomalies on pentad intervals than monthly. Overall, the discrepancy is greatest during JJA, especially over the monsoon region and the southeastern United States. During SON there is a peak along the coastlines of the southern Gulf of Mexico, coincident with the season of frequent tropical storm landfall in that region. The minimum impact is during DJF for most regions, although over the Northwest the discrepancies are large in all seasons.

5. Discussion

The quasi-isentropic back trajectory scheme of Brubaker et al. (2001) has been applied to data from MERRA. Estimates of the surface evaporative sources of moisture supplying precipitation over land for the period 1979-2005 are presented. Results are consistent with previous analyses (e.g., Brubaker et al. 2001; Dirmeyer and Brubaker 2007, Dirmeyer and Kinter 2010), but the higher spatial resolution of the MERRA data set reveals more structure. Systematic biases in MERRA precipitation have a large effect on the surface water budget, which also impact the estimates of evaporative sources. Thus, precipitation estimates have been corrected using gridded data from GPCP, and evaporation data come from the MERRA-Land offline replay also driven by observationally-based precipitation.

The methodology allows for estimates of moisture recycling and the partitioning of local precipitation between terrestrial and oceanic sources, as well as estimates of the distance over which moisture typically travels in the atmosphere prior to falling as precipitation over any location. Recognizing that the two-dimensional distributions of evaporative moisture source are tantamount to probability distributions, we have used the statistical metric of relative entropy to compare evaporative sources for any region under different conditions; namely cases of drought or flood based on local precipitation anomalies.

We find that changes in local and remote surface evaporative sources of moisture supplying precipitation over land are more a factor behind droughts than wet anomalies over most regions of the globe. Examining results grouped by season, much of the globe shows significant differences in evaporative moisture sources for

381 the driest ~10% (3 out of 27) of the time periods. On the other hand, very little area
382 appears to pass significance tests for comparable wet anomalies. Some of this
383 discrepancy is due to the difference in time scales underpinning droughts and floods
384 – when pentad data are considered instead of monthly data, relative entropy
385 estimates for floods increase.

386 The finding that droughts are more strongly tied to changes in evaporative sources
387 than floods seems to run counter to previous findings with this method linking
388 floods to anomalous advection of moisture (e.g., Dirmeyer et al. 1999; Reale et al.
389 2001; Turato et al. 2004; Dirmeyer and Kinter 2009, 2010), and more generally the
390 link between "atmospheric rivers" and extreme precipitation events. It may be that
391 our screening for the wettest years conflates such cases with extreme rainfall events
392 that have more localized causes. In this study, we have not tried to identify specific
393 cases of atmospheric rivers as those previous studies did. Rather, we conditioned
394 the data based simply on a ranking of precipitation amounts.

395 To try to discern whether there is more of a change in moisture transport for
396 droughts than floods, we revisit the metric shown in Fig 4 – mean distance to the
397 evaporative source. Distances to the center of mass of evaporative sources have
398 been calculated for the three wettest and driest years for each month, the same
399 cases as in Figs 5 and 6, and then averaged for seasons. The differences in the mean
400 distances (wet minus dry), expressed as a percentage of the 27-year climatological
401 mean distance to evaporative source, are shown in Fig 10. On average, distances to
402 moisture sources are greater during droughts than wet periods – as much as 12%
403 during SON for the global mean. Distances are actually greater, averaged globally,

for both extremes, but the differences from climatology for wet cases are less than half that for droughts on average. The figure shows that there are significant regional variations. Semi-arid and arid regions, where precipitable moisture often has a relatively long path, generally have more distant fetches during droughts than wet intervals (blue shading). This may reflect the near-total lack of evaporation in the drought regions, meaning any moisture must come from relatively farther away. When conditions are wet, there can be excess local evaporation. Indeed, calculations of the difference between wet conditions and climatology (not shown) indicate moisture transport distances are shorter over arid zones.

Previous studies have suggested that floods over the eastern United States may tap more distant sources of moisture from the Caribbean Sea (e.g., Brubaker et al. 2001; Dirmeyer and Kinter 2010), and Fig 10 supports that conclusion. Yet we do not see a similar signal for California and the West coast in winter, where long "atmospheric rivers" are often implicated in floods. Other red shaded regions also tap more distant moisture sources during wet periods than dry.

Significant changes in evaporative moisture sources found in this analysis during times of drought could have several causes. The calculation of evaporative sources depends not only on the atmospheric circulation (horizontal wind field), but also on column integrated precipitable water and surface evaporation rates, which are used to determine the contribution of each upstream grid box to the overall moisture supply for downstream precipitation. In this study, we have not attempted to differentiate between these dynamical and hydrological factors, and even in Fig 10 they remain conflated.

427 Furthermore, a lack of significant contribution to precipitation extremes from
428 changing moisture transport, estimated using relative entropy, does not indicate
429 what other phenomena may be the cause. Alternative factors may include local
430 increases in atmospheric stability (buoyancy or shear), regional changes such as
431 large-scale subsidence, increased entrainment of dry air at the top of an otherwise
432 favorable boundary layer, or a change in coupled land-atmosphere feedbacks caused
433 by anomalous land surface conditions. Further diagnoses would be helpful to better
434 understand the combination of events that contribute to precipitation extremes
435 around the globe.

436 *Acknowledgements:* This research was supported by National Aeronautics and Space
437 Administration grant NNX09AI84G.

438

439 **References:**

440 Bagley, J. E., A. R. Desai, P. A. Dirmeyer, and J. A. Foley, 2012: Effects of land cover
441 change on precipitation and crop yield in the world's breadbaskets. Env. Res.
442 Lett., 7, 014009, doi: 10.1088/1748-9326/7/1/014009.

443 Bisselink, B., and A. J. Dolman, 2008: Precipitation recycling: Moisture sources over
444 Europe using ERA-40 data. J. Hydrometeor., 9, 1073-1083.

445 Bosilovich, M. G., and W.-Y. Sun, 1999: Numerical simulation of the 1993
446 midwestern flood: Local and remote sources of water. J. Geophys. Res., 104,
447 19415-19423.

448 Bosilovich, M. G., and S. D. Schubert, 2002: Water vapor tracers as diagnostics of the
449 regional hydrologic model. J. Hydrometeor., 3, 149-165.

450 Brubaker, K. L., D. Entekhabi, and P. S. Eagleson, 1993: Estimation of continental
451 precipitation recycling. *J. Climate*, **6**, 1077-1089.

452 Brubaker, K. L., P. A. Dirmeyer, A. Sudradjat, B. Levy, and F. Bernal, 2001: A 36-year
453 climatology of the evaporative sources of warm-season precipitation in the
454 Mississippi River Basin. J. Hydrometeor., 2, 537-557.

455 Budyko, M. I., , 1974: . Climate and Life, Academic Press, New York, 508 pp.

456 Burde, G. I., A. Zangvil, and P. J. Lamb, 1996: Estimating the role of local evaporation
457 in precipitation for a two-dimensional region. J. Climate, 9, 1328-1338.

458 Burde, G. I., and A. Zangvil, 2001: The estimation of regional precipitation recycling.
459 Part II: A new recycling model. J. Climate, 14, 2509-2527.

460 Decker, M., M. Brunke, Z. Wang, K. Sakaguchi, X. Zeng, and M.G. Bosilovich, 2012:
461 Evaluation of the reanalysis products from NCEP, ECMWF, and NASA using flux
462 tower observations. J. Climate, 25, 1916-1944, doi:10.1175/JCLI-D-11-00004.1.

463 DelSole, T., and M. K. Tippett, 2007: Predictability: Recent insights from information
464 theory. Rev. Geophys., 45, RG4002.

465 Dettinger, M. D., F. M. Ralph, T. Das, P. J. Neiman, and D. Cayan, 2011: Atmospheric
466 rivers, floods, and the water resources of California. Water, 3, 455-478.

467 Dirmeyer, P. A., and K. L. Brubaker, 1999: Contrasting evaporative moisture sources
468 during the drought of 1988 and the flood of 1993. J. Geophys. Res., 104, 19383-
469 19397.

470 Dirmeyer, P. A., and K. L. Brubaker, 2007: Global characterization of the hydrologic
471 cycle from a quasi-isentropic back-trajectory analysis of atmospheric water
472 vapor. J. Hydrometeor. 8, 20-37.

473 Dirmeyer, P. A., K. L. Brubaker, and T. DelSole, 2009: Import and export of
474 atmospheric water vapor between nations. J. Hydrol., 365, 11-22.

475 Dirmeyer, P. A., and J. L. Kinter III, 2009: The Maya Express - Late spring floods in
476 the US Midwest. Eos – Transactions of the American Geophysical Union, 90, 101-
477 102.

478 Dirmeyer, P. A., and J. L. Kinter III, 2010: Floods over the US Midwest: A regional
479 water cycle perspective. J. Hydrometeor., 11, 1172-1181.

480 Dirmeyer, P. A., 2011: The terrestrial segment of soil moisture-climate coupling.
481 Geophys. Res. Lett., 38, L16702, doi: 10.1029/2011GL048268.

Dominguez, F., P. Kumar, X.-Z. Liang, and M. Ting, 2006: Impact of atmospheric moisture storage on precipitation. J. Climate, 19, 1513-1530.

Druyan, L. M., and R. D. Koster, 1989: Sources of Sahel precipitation for simulated drought and rainy seasons. J. Climate, 2, 1438-1446.

Ducharne, A., R. D. Koster, M. J. Suarez, M. Stieglitz, and P. Kumar, 2000: A catchment-based approach to modeling land surface processes in a general circulation model, 2, Parameter extimation and model demonstration. J. Geophys. Res., 105, 24823-24838.

Eltahir, E. A. B., and R. L. Bras, 1994: Precipitation recycling in the Amazon Basin. Quart. J. Roy. Meteor. Soc., 120, 861-880.

Gimeno, L., A. Drumond, R. Nieto, R. M. Trigo, and A. Stohl, 2010: On the origin of continental precipitation. Geophys. Res. Lett., 37, L13804, doi: 10.1029/2010GL043712.

Gimeno, L., A. Stohl, R. M. Trigo, F. Dominguez, K. Yoshimura, L. Yu, A. Drumond, A. M. Durán-Quesada, and R. Nieto, 2012: Oceanic and terrestrial sources of continental precipitation. Rev. Geophys., 50, RG4003, doi: 10.1029/2012RG000389.

Goessling, H. F. and C. H. Reick, 2011: What do moisture recycling estimates tell us? Exploring the extreme case of non-evaporating continents. Hydrol. Earth Syst. Sci., 15, 3217-3235, doi: 10.5194/hess-15-3217-2011.

Gong, C., and E. Eltahir, 1996: Sources of moisture for rainfall in West Africa. Water Resour. Res., 32, 3115-3121.

504 Henderson-Sellers, A., K. McGuffie, D. Noone, and P. Irannejad, 2004: Using stable
505 water isotopes to evaluate basin-scale simulations of surface water budgets. J.
506 Hydrometeor., 5, 805-822.

507 Huffman, G. J., R. F. Adler, D. T. Bolvin, and G. Gu, 2009: Improving the global
508 precipitation record: GPCP Version 2.1, Geophys. Res. Lett., 36, L17808,
509 doi:10.1029/2009GL040000.

510 Kanamitsu, M., W. Ebisuzaki, J. Woollen, S.-K. Yang, J. J. Hnilo, M. Fiorino, and G. L.
511 Potter, 2002: NCEP-DOE AMIP-II reanalysis (R-2). Bull. Amer. Meteor. Soc., 83,
512 1631-1648.

513 Keys, P. W., R. J. van der Ent, L. J. Gordon, H. Hoff, R. Nikoli, and H. H. G. Savenije,
514 2012: Analyzing precipitationsheds to understand the vulnerability of rainfall
515 dependent regions. Biogeosci., 9, 733-746.

516 Kleeman, R., 2002: Measuring dynamical prediction utility using relative entropy. J.
517 Atmos. Sci., 59, 2057-2072.

518 Koster, R. D., M. J. Suarez, A. Ducharne, M. Stieglitz, and P. Kumar, 2000: A
519 catchment-based approach to modeling land surface processes in a general
520 circulation model, 1, Model structure. J. Geophys. Res., 105, 24809-24822.

521 Kurita, N., N. Yoshida, G. Inoue, and E. A. Chayanova, 2004: Modern isotope
522 climatology of Russia: A first assessment. J. Geophys. Res., 109, D03102, doi:
523 10.1029/2003JD003404.

524 Numaguti, A., 1999: Origin and recycling processes of precipitating water over the
525 Eurasian continent: Experiments using an atmospheric general circulation model.
526 J. Geophys. Res., 104, 1957-1972.

527 Reale, O., L. Feudale, and B. Turato, 2001: Evaporative moisture sources during a
528 sequence of floods in the Mediterranean region. Geophys. Res. Let., 28, 2085-
529 2088.

530 Reichle, R. H., R. D. Koster, G. J. M. De Lannoy, B. A. Forman, Q. Liu, S. P. P. Mahanama,
531 and A. Touré, 2011: Assessment and enhancement of MERRA land surface
532 hydrology estimates. J. Climate, 24, 6322–6338.

533 Rienecker, M. M., and Coauthors, 2011: MERRA: NASA's Modern-Era Retrospective
534 Analysis for Research and Applications. J. Climate, 24, 3624–3648.

535 Robertson, F. R., M. Bosilovich, J. Chen, and T. Miller, 2011: The effect of satellite
536 observing system changes on MERRA water and energy fluxes. J. Climate, 24,
537 5197-5217, doi:10.1175/2011JCLI4227.1.

538 Salati, E., A. Dall'Olio, E. Matsui, and J. Gat, 1979: Recycling of water in the Amazon
539 Basin: an isotopic study. Water Resour. Res., 15, 1250-1258.

540 Spracklen, D. V., S. R. Arnold, and C. M. Taylor, 2012: Observations of increased
541 tropical rainfall preceded by air passage over forests. Nature, 489, 282-286.

542 Stohl, A. and P. James, 2004: A Lagrangian analysis of the atmospheric branch of the
543 global water cycle. Part I: Method description, validation, and demonstration for
544 the August 2002 flooding in Central Europe. J. Hydrometeor., 5, 656-678.

545 Stohl, A. and P. James, 2005: A Lagrangian analysis of the atmospheric branch of the
546 global water cycle. Part II: Moisture transport between earth's ocean basins and
547 river catchments. J. Hydrometeor., 6, 961-984.

548 Sudradjat, A., 2002: Source-sink analysis of precipitation supply to large river
549 basins. PhD Dissertation, [Available from University of Maryland, College Park,
550 MD 20742, U.S.A.], 186 pp.

551 Sudradjat, A., K. L. Brubaker, and P. A. Dirmeyer, 2003: Interannual variability of
552 surface evaporative moisture sources of warm-season precipitation in the
553 Mississippi River Basin.. J. Geophys. Res., 108, doi: 10.1029/2002JD003061.

554 Tian, L., V. Masson-Delmotte, M. Stievenard, T. Yao, and J. Jouzel, 2001: Tibetan
555 Plateau summer monsoon northward extent revealed by measurements of water
556 stable isotopes. J. Geophys. Res., 106, 28081-28088.

557 Trenberth, K. E., 1999: Atmospheric moisture recycling: Role of advection and local
558 evaporation. J. Climate, 12, 1368-1381.

559 Tuinenburg, O. A. , R. W. A. Hutjes, and P. Kabat, 2012: The fate of evaporated water
560 from the Ganges basin. J. Geophys. Res., 117, D01107, doi:
561 10.1029/2011JD016221.

562 Turato, B., O. Reale, and F. Siccardi, 2004: Water vapor sources of the October 2000
563 Piedmont flood. J. Hydrometeor., 5, 693-712.

564 van der Ent, R. J., H. H. G. Savenije, B. Schaefli, and S. C. Steele-Dunne, 2010: Origin
565 and fate of atmospheric moisture over continents. Water Resour. Res., 46,
566 W09525, doi: 10.1029/2010WR009127.

567 Wei, J., P. A. Dirmeyer, M. J. Bosilovich, and R. Wu. 2012: Water vapor sources for
568 Yangtze River Valley rainfall: Climatology, variability, and implications for rainfall
569 forecasting, J. Geophys. Res., 117, D05126, doi:10.1029/2011JD016902.

570 Wei, J., P. A. Dirmeyer, D. Wisser, M. J. Bosilovich, and D. M. Mocko, 2013: Where
571 does the irrigation water go? An estimate of the contribution of irrigation to
572 precipitation using MERRA. J. Hydrometeor., 14, 275-289, doi: 10.1175/JHM-D-
573 12-079.1.

574 Xie, P., J. E. Janowiak, P. A. Arkin, R. Adler, A. Gruber, R. Ferraro, G. J. Huffman, and S.
575 Curtis , 2003: Gauge-based monthly analysis of global land precipitation from
576 1971 to 1994. J. Climate, 16, 2197-2214.

577 Yoshimura, K., T. Oki, N. Ohte, and S. Kanae, 2004: Colored moisture analysis
578 estimates of variations in 1998 Asian monsoon water sources. J. Meteor. Soc.
579 Japan, 82, 1315–1329.

580

Figure Captions:

Figure 1. Top panels: total seasonal evaporative source (kg m^{-2}) for all precipitation over ice-free land based on MERRA atmospheric data with MERRA-Land evaporation and precipitation estimates. Bottom panels: Difference when all data from MERRA are used instead.

Figure 2: 27-year mean evaporative source for precipitation over the outlined states, expressed as the fraction of total originating from each MERRA grid box (normalized so the global sum for each equals 1). The two contours represent 50 and 100 parts per million, shading indicates greater than 200 and 300 parts per million.

Figure 3: Fraction of precipitation originating as evaporation over land.

Figure 4: Distance to the center of mass of the mean evaporative source distribution for each land grid point (km) for DJF (top) and JJA (bottom).

Figure 5: The average relative entropy at each point calculated between the climatological evaporative moisture source and the source for each of the 27 years. Large values indicate greater interannual variability in the source of moisture supplying local precipitation.

Figure 6. Relative entropy between the climatological evaporative source distribution and the evaporative source distribution for the three driest years, calculated for each ice-free land grid point using monthly data and then averaged for each season. Regions with climatological rainfall rates less than 0.1 mm/day

602 are masked. Areas where the relative entropy is not significant at the 90%
603 confidence level are shaded dark grey.

604 Figure 7. As in Fig 6, for the wettest three years.

605 Figure 8. As in Fig 7, but calculated using pentad instead of monthly data. No
606 significance screening has been applied.

607 Figure 9. The natural logarithm of the ratio of the relative entropy calculated with
608 pentad data over that calculated with monthly data.

609 Figure 10: Difference (three wettest minus three driest years) in the average
610 distance between precipitation at each land point and the evaporative source
611 supplying that precipitation, expressed as a percentage of the climatological
612 average distance. Positive values indicate dry conditions have closer moisture
613 sources than wet.

614

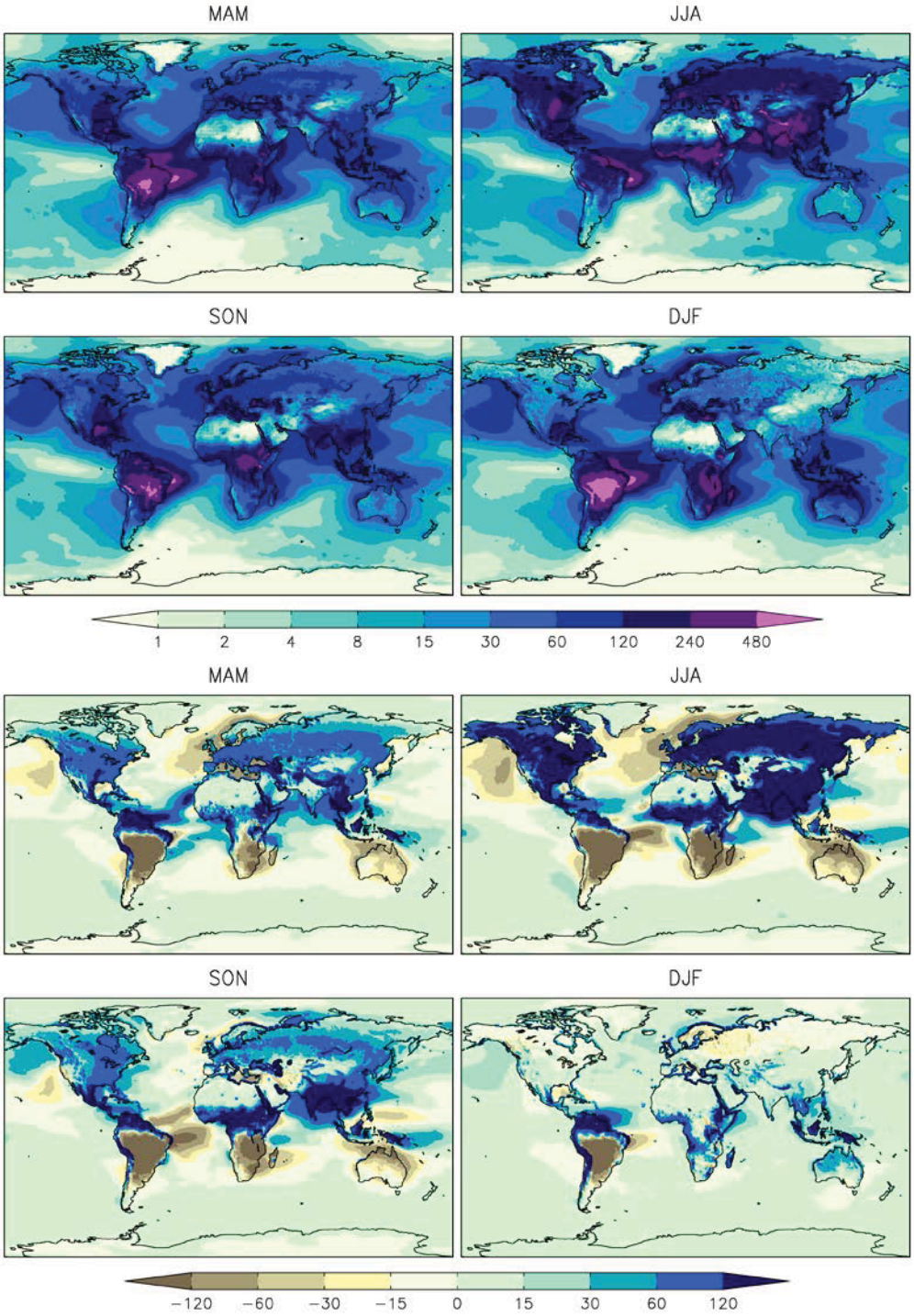

615 Figure 1. Top panels: total seasonal evaporative source (kg m^{-2}) for all precipitation
616 over ice-free land based on MERRA atmospheric data with MERRA-Land
617 evaporation and precipitation estimates. Bottom panels: Difference when all data
618 from MERRA are used instead.

619

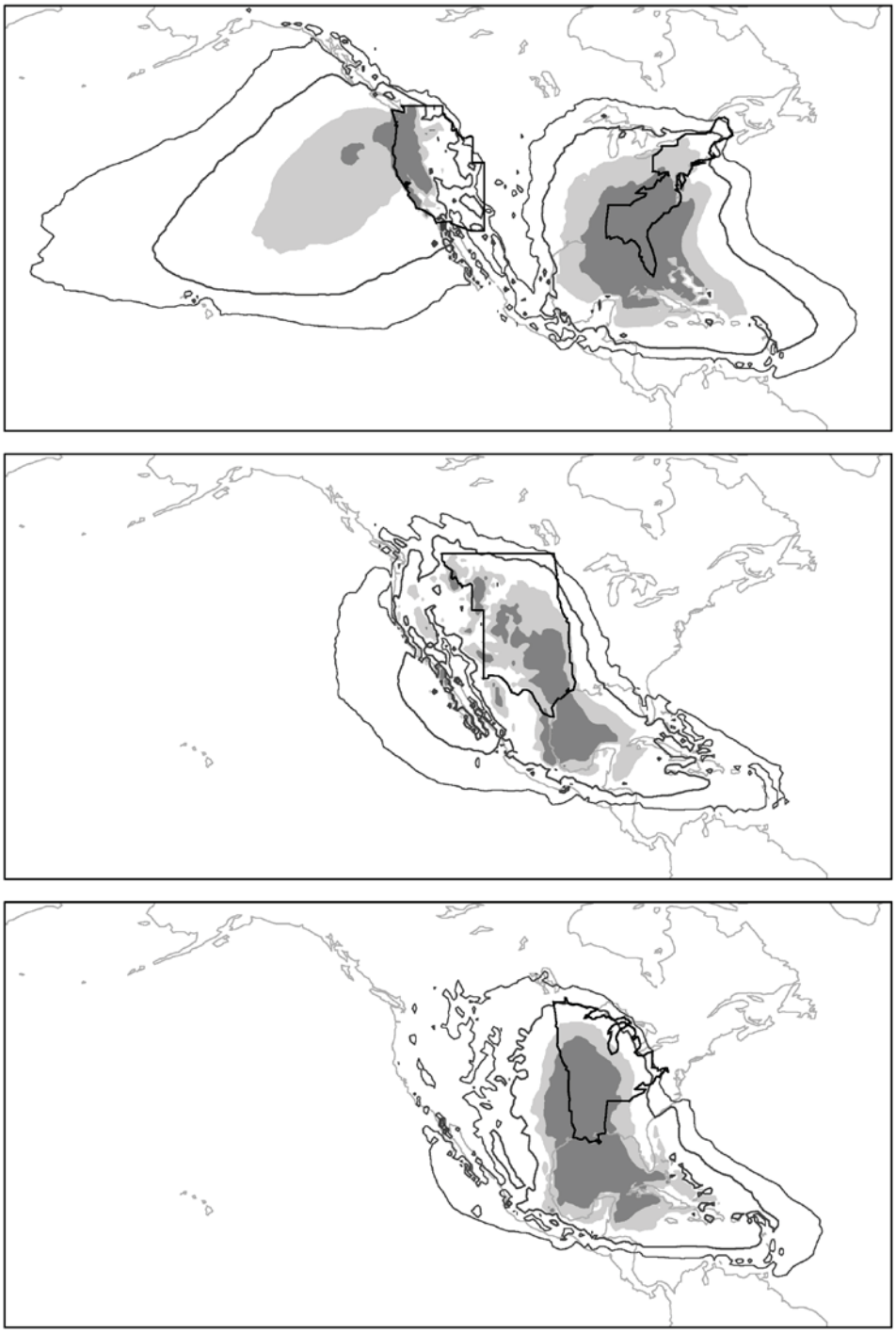

Figure 2: 27-year mean evaporative source for precipitation over the outlined states, expressed as the fraction of total originating from each MERRA grid box (normalized so the global sum for each equals 1). The two contours represent 50 and 100 parts per million, shading indicates greater than 200 and 300 parts per million.

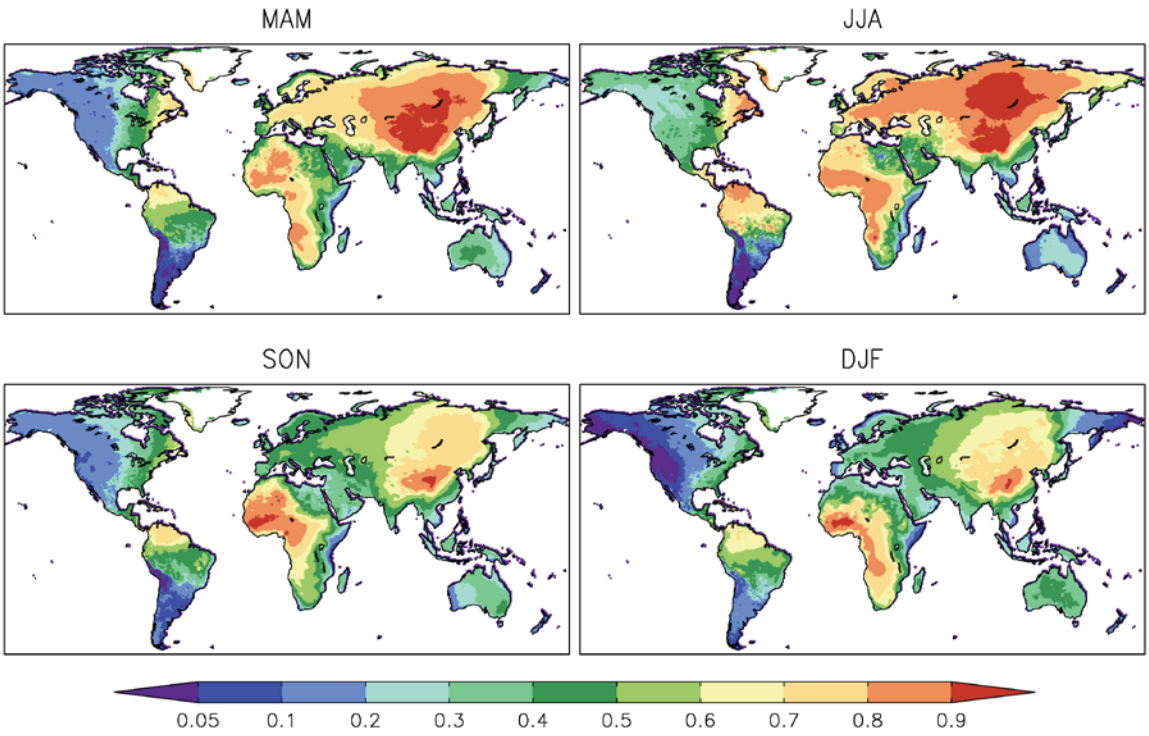

627

628 Figure 3: Fraction of precipitation originating as evaporation over land.

629

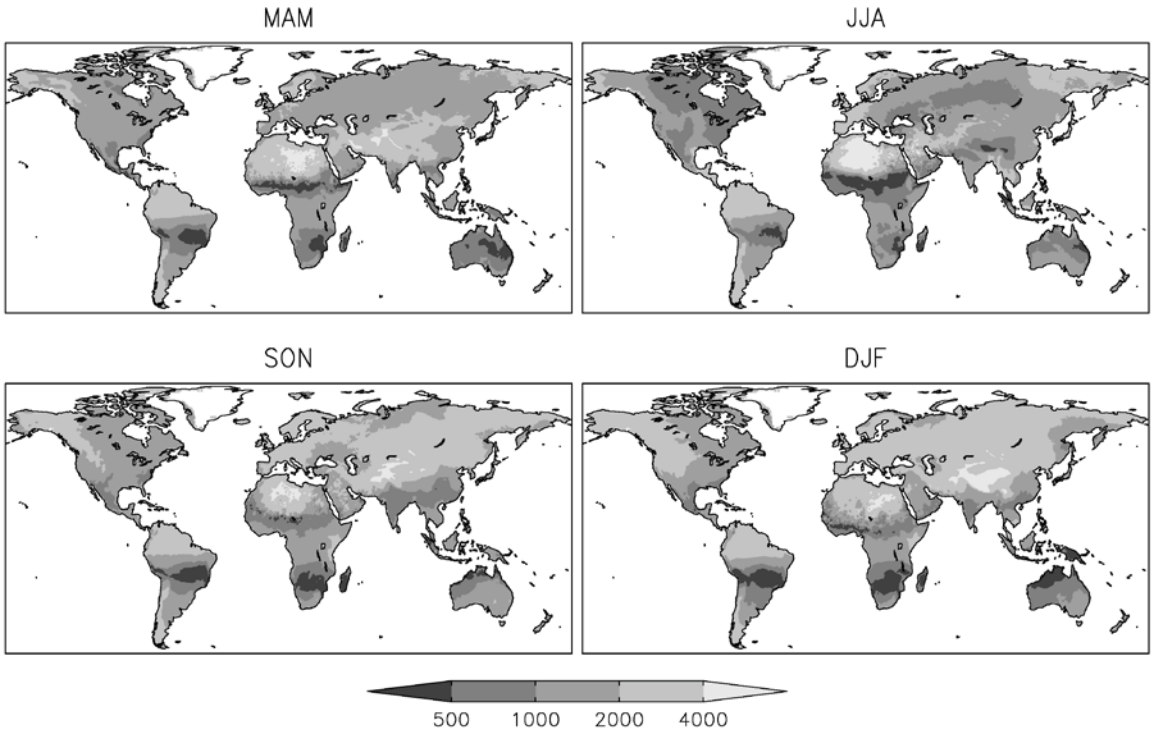

630 Figure 4: Distance to the center of mass of the mean evaporative source distribution
631 for each land grid point (km).

632

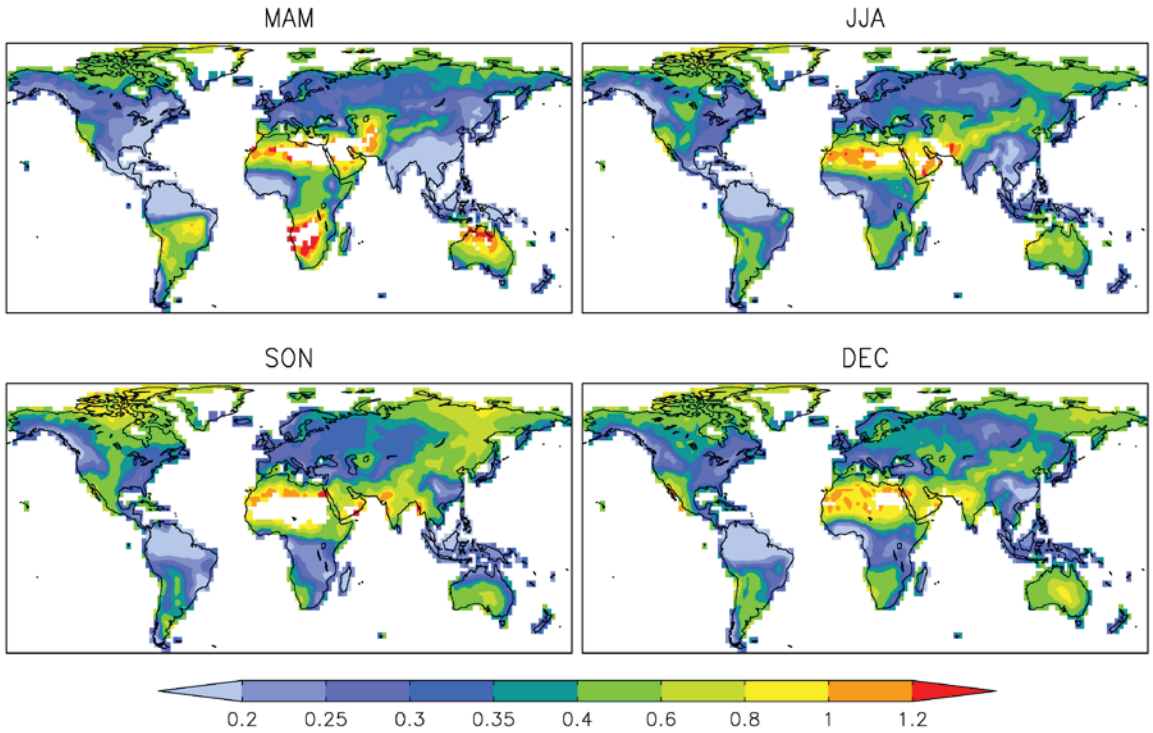

633 Figure 5: The average relative entropy at each point calculated between the
634 climatological evaporative moisture source and the source for each of the 27
635 years. Large values indicate greater interannual variability in the source of
636 moisture supplying local precipitation.

637

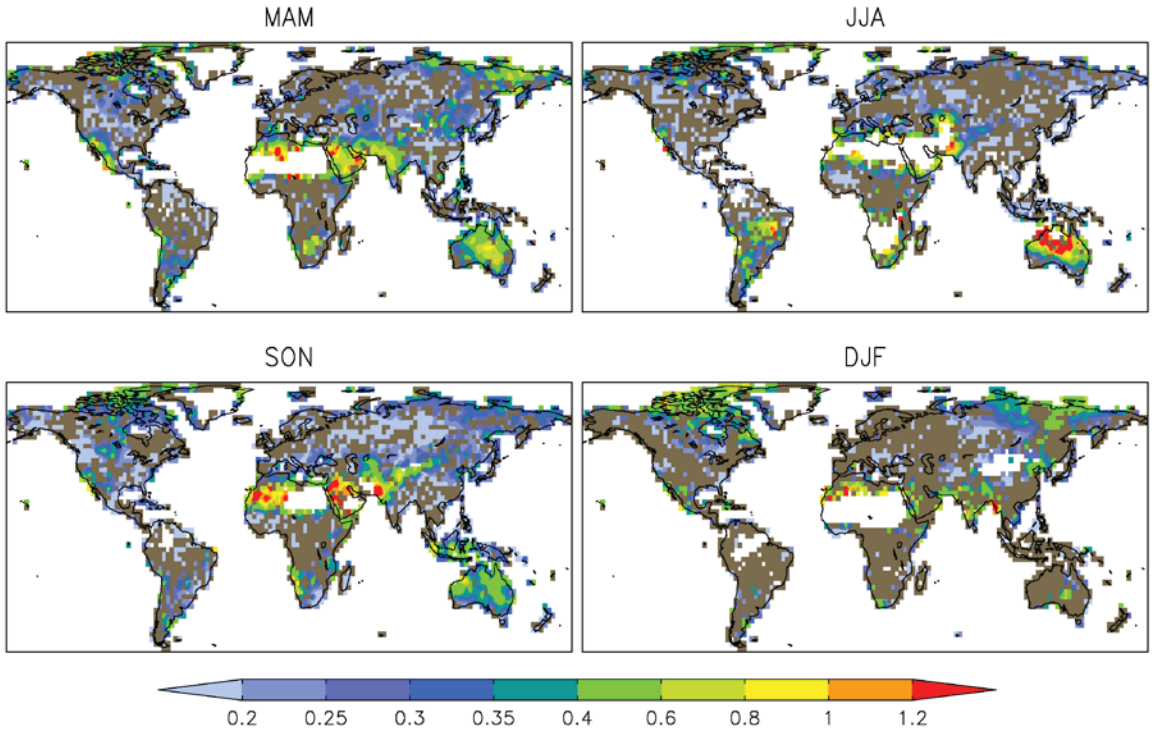

638

639 Figure 6. Relative entropy between the climatological evaporative source
640 distribution and the evaporative source distribution for the three driest years,
641 calculated for each ice-free land grid point using monthly data and then averaged
642 for each season. Regions with climatological rainfall rates less than 0.1 mm/day
643 are masked. Areas where the relative entropy is not significant at the 90%
644 confidence level are shaded dark grey.

645

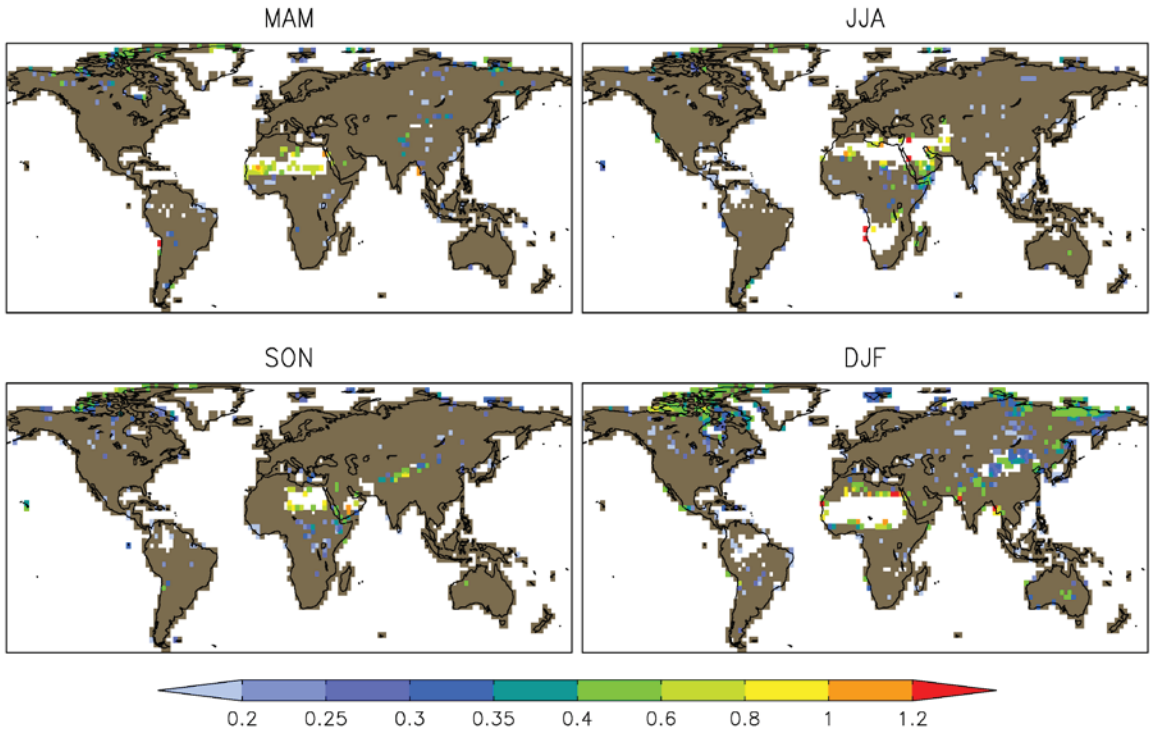

646 Figure 7. As in Fig 6, for the wettest three years.

647

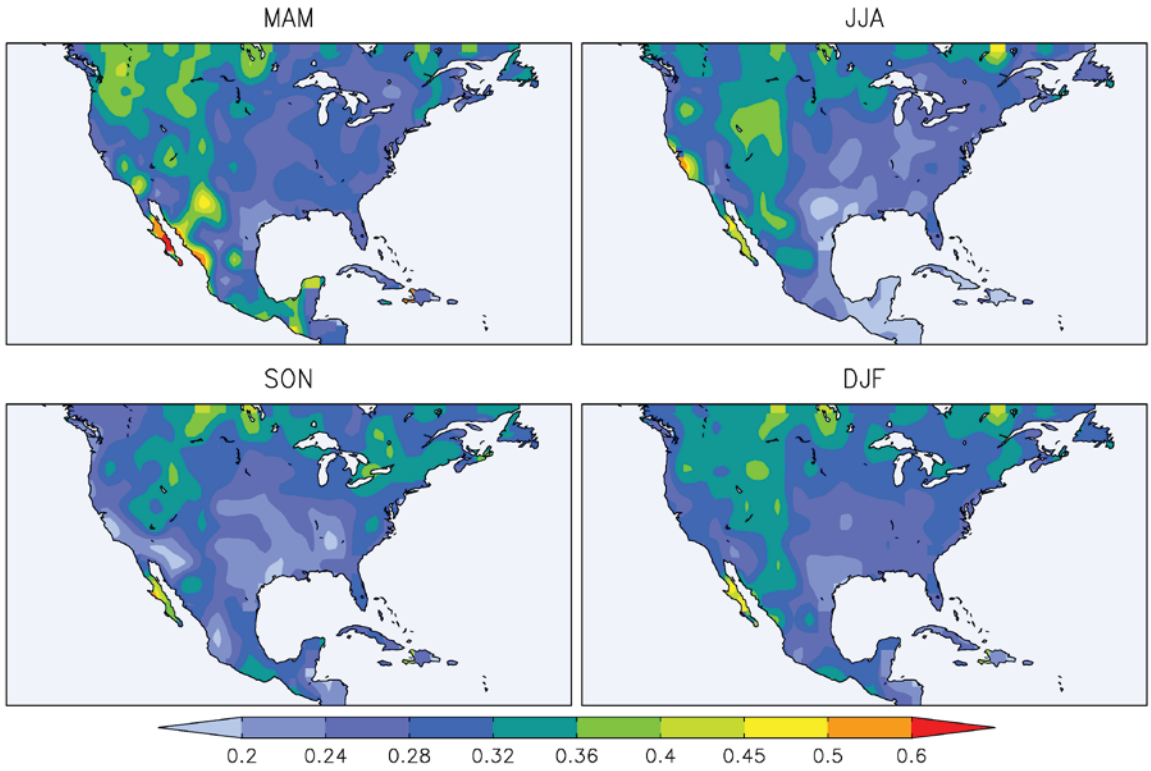

Figure 8. As in Fig 7, but calculated using pentad instead of monthly data. No significance screening has been applied.

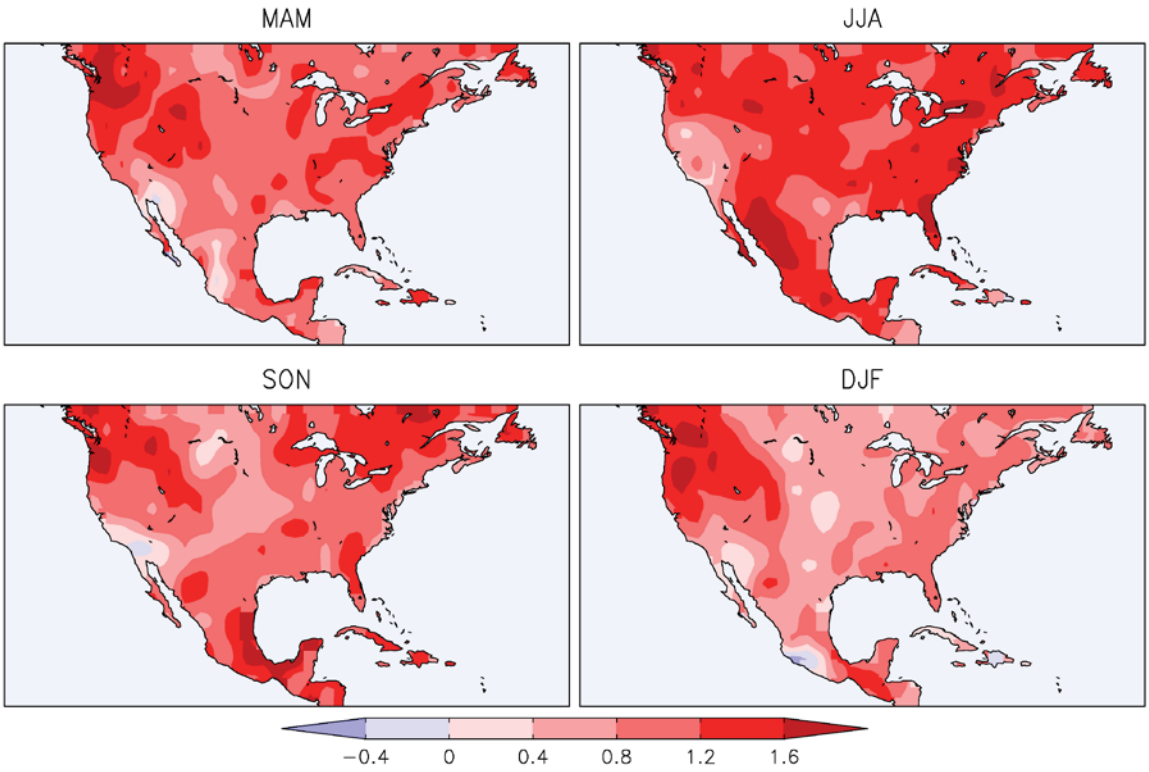

652

653 Figure 9. The natural logarithm of the ratio of the relative entropy calculated with
654 pentad data over that calculated with monthly data.

655

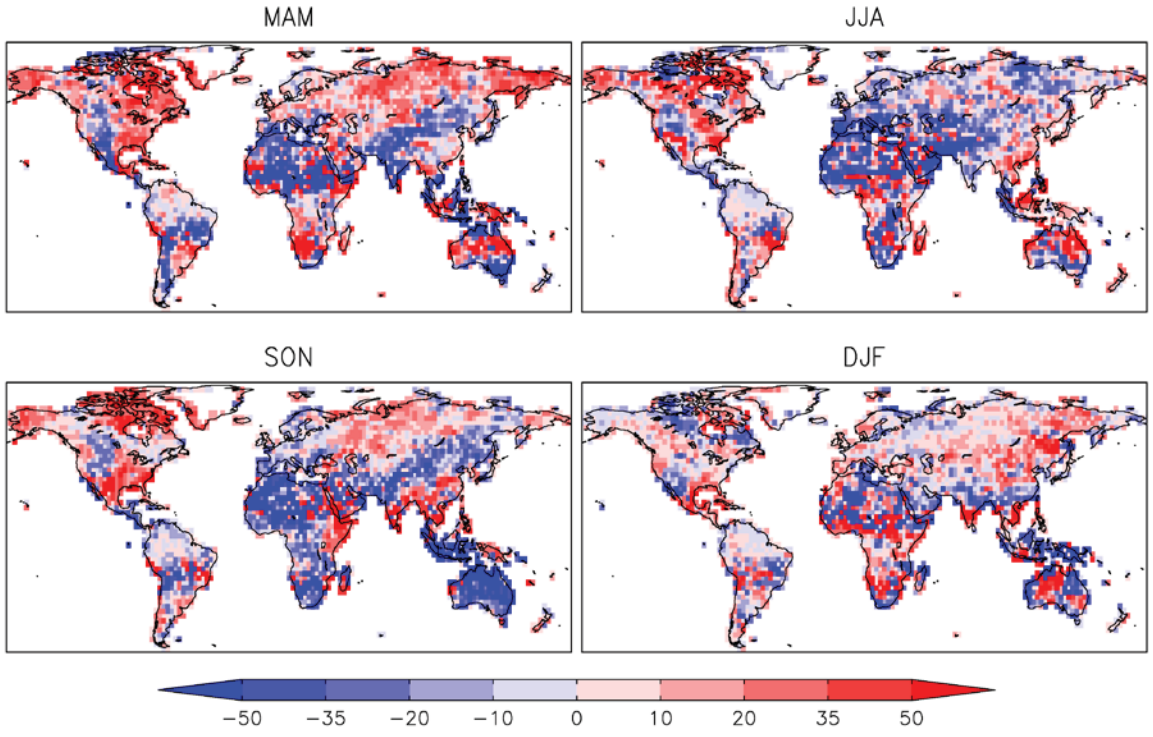

Figure 10: Difference (three wettest minus three driest years) in the average distance between precipitation at each land point and the evaporative source supplying that precipitation, expressed as a percentage of the climatological average distance. Positive values indicate dry conditions have closer moisture sources than wet.